Sedimentological characterization of earthquake-generated turbidites in fault-proximal glacial lakes: a case study from Jenny Lake, Teton range, Wyoming

Darren J. Larsen[1]*, Aria R. Blumm[1], Sarah E. Crump[2],
Amelia P. Muscott[2], Mark B. Abbott[3], Alexandra Hangsterfer[4]
and Maya Porcelli[1]

[1]Department of Geology, Occidental College, Los Angeles, CA, United States, [2]Department of
Geology and Geophysics, University of Utah, Salt Lake City, UT, United States, [3]Department of
Geology and Environmental Science, University of Pittsburgh, Pittsburgh, PA, United States, [4]Scripps
Institution of Oceanography, UC San Diego, La Jolla, CA, United States

Lakes in seismically active regions preserve valuable sedimentary archives of paleoseismic activity within their catchment and beyond. A series of glacially-excavated lakes positioned directly along the surface trace of the Teton normal fault at the base of the Teton Range, WY, are ideally situated to record past fault activity since their formation approximately 15,000 years ago. Here, we focus on the sediment fill contained in Jenny Lake (5 km^2; approximately 73 m max depth) located at the bottom of Cascade Canyon, in the central Tetons, where postglacial slip rates are greatest. Past earthquakes that generated slope failures in and around Jenny Lake are expressed stratigraphically as coseismic turbidite deposits. These deposits were previously identified and dated in sub-bottom profiles and in sediment cores taken from multiple locations around the basin. In this study, we focus on the six thickest turbidites (ranging from 6 to 34 cm thick) present in multiple cores recovered from the central depositional basin and analyze them at sub-centimeter resolution for changes in physical, biological, and geochemical parameters, including sediment density, magnetic susceptibility, grain size distributions, organic content, and elemental composition. Results reveal each deposit contains a well-defined, three-component sedimentary sequence composed of a relatively homogenous and thick basal sandy unit with a sharp bottom contact, a similarly thick silt-rich middle unit, and a thin top unit of very fine-grained sediments. The characteristics of these components and their similarity between individual deposits suggest consistent sediment sources and transport pathways during successive earthquake events. Based on our analyses and the unique local geomorphic setting, we create a mechanistic model of coseismic turbidite formation in Jenny Lake, which may provide an

improved framework for identifying, characterizing, and correlating earthquake-generated disturbance deposits in other Teton lakes and lakes in similar tectonic-geomorphological settings, for example, in the Basin and Range Province, USA or beyond.

1 Introduction

Paleoseismic histories derived from lacustrine sediments have become increasingly common for determining past seismic activity near major plate boundaries (e.g., Howarth et al., 2012; Morey et al., 2013; Moernaut, et al., 2014; 2017; 2018; Leithold et al., 2019; Van Daele et al., 2019; Praet et al., 2020) and in intra-plate settings (e.g., Strasser et al., 2006; 2007; 2013; Beck, 2009; Maloney et al., 2013; Smith et al., 2013; Larsen et al., 2019; Fan et al., 2022). Lakes in these regions can preserve indirect evidence of past earthquakes due to coseismic shaking, which mobilizes and reworks sediment in the lake and its catchment, and results in diagnostic deposits in the sediment stratigraphy. The expressions of such disturbance beds are not uniform and are dependent on a large variety of factors, including the size and shape of the lake basin and the geomorphic relation to active faults in the region. For example, shallow lakes with gently sloping sides often record seismic shaking events as soft sediment deformation, microfaulting, and/or liquefaction structures, while deep lakes in steep-sided basins document strong ground shaking events as turbidite, debris flow, and/or slump deposits (e.g., Becker et al., 2005; Sabatier et al., 2022). The ability to construct continuous, precisely-dated, and temporally long paleoseismic histories from lakes makes them strong complements to other paleoseismic methods, such as fault scarp trench exposures, which can provide more direct evidence of surface rupturing earthquakes (including rupture age and surface displacement), but which can be discontinuous and/or temporally restricted to recent rupture events and typically have large dating uncertainties (e.g., Byrd et al., 1994; DuRoss et al., 2020). However, because 1) seismically-generated deposits in lakes differ depending on the tectonic-geomorphic setting, and 2) deposits from other extreme events like floods can have similar characteristics, a detailed characterization of coseismic lacustrine turbidites are required in order to establish reliable paleoseismic histories from a given location.

The goal of this study is to characterize earthquake-generated turbidites in fault-proximal, steep-sided, glacially-excavated lake basins such as those present in the Basin and Range Province, USA and elsewhere. We analyze the sedimentological and geochemical composition of seismically-generated deposits in a well-constrained lake setting in the Teton Range, WY, where a series of moraine-dammed piedmont lakes along the eastern range front are located at the mouths of their respective glacial valleys and positioned directly along the range-bounding Teton normal fault (Figure 1). Sediment fill in these lakes preserves a continuous and datable record of postglacial landscape evolution, including past earthquake events, which are registered as distinctive turbidite deposits that can be confidently identified and correlated to the timing of surface

rupturing earthquakes dated in fault trenches (Larsen et al., 2016; 2019). We leverage this well-constrained system to conduct a detailed study of the most prominent turbidite deposits at Jenny Lake and to develop a better understanding of the stratigraphic expression of past earthquake events in Teton lake sediment archives. We also present a mechanistic model for turbidite formation in Teton lakes, including the interplay between subaqueous slope failures and proximal landslides, as well as features that distinguish coseismic turbidites from those formed by other processes.

2 Geological setting

2.1 The Teton fault

2.1.1 Tectonic setting

The Teton fault is an approximately 72-km-long, north-south striking, eastward-dipping normal fault that accommodates intra-plate extension in the northeastern Basin and Range Province (Machette et al., 2001; Zellman et al., 2019) (Figure 1). Fault displacement during the past approximately 15,000 years is recorded by prominent fault scarps that displace glacier deposits from the most recent (Pinedale) glaciation (Figure 1; Pierce et al., 2018; Licciardi and Pierce, 2018; Zellman et al., 2019). In general, vertical surface offsets of glacial and colluvial landforms are greatest in the central portion of the fault, where they exceed 25 m in the region near Jenny Lake and decrease to approximately 10 m toward the northern and southern ends (Hampel et al., 2021). Based on these surface offsets and the attendant landform ages, relatively high time-averaged postglacial slip rates of approximately 1.8 mm/yr and approximately 0.9 mm/yr have been inferred for the central and distal portions of the fault, respectively (Thackray and Staley, 2017; Hampel et al., 2021).

2.1.2 Postglacial paleoseismicity

Previous investigations suggest the cumulative postglacial fault offset occurred through a series of 7–10 discrete rupture events (e.g., Pierce and Good, 1992; Smith et al., 1993; Byrd et al., 1994; White et al., 2009; Larsen et al., 2019). Information on past rupture events comes primarily from trench excavations and lake sediment studies. To date, trench excavations have been performed at five locations along the fault: Ski Lake (Zellman et al., 2020a), Buffalo Bowl (DuRoss et al., 2019), Granite Canyon (Byrd et al., 1994; Byrd, 1995), Leigh Lake (Zellman et al., 2020b), and Steamboat Mountain (DuRoss et al., 2020) (Figure 1). Together, the trench datasets provide evidence for at least three surface rupturing earthquakes of the Teton fault at approximately 10 ka, approximately 8 ka, and approximately 5 ka (see summary in DuRoss et al., 2020).
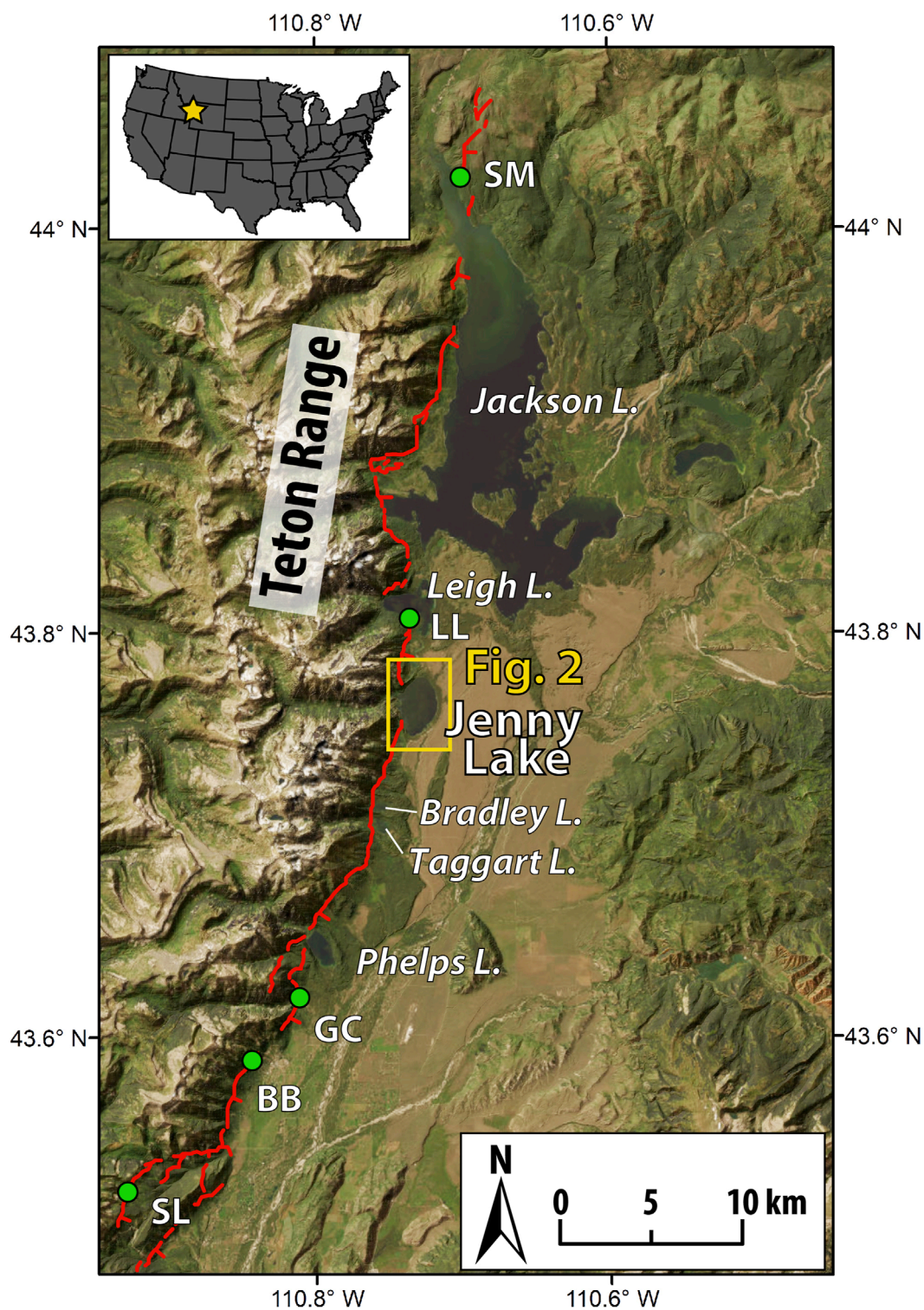
FIGURE 1
Overview map of the Teton Range. The generalize surface trace of the Teton normal fault system is shown (red line) along the eastern range-front (fault data from USGS Quaternary fault and fold database and modified from Zellman et al. (2019)). A series of moraine-impounded lakes are positioned along the fault trace: Phelps Lake, Taggart Lake, Bradley Lake, Jenny Lake (this study), Leigh Lake, and Jackson Lake. In many cases, the fault cuts across the lake inflow deltas. The location of paleoseismic trench studies are shown (green dots) and include Ski Lake (SL; Zellman et al., 2020a), Buffalo Bowl (BB; DuRoss et al., 2019), Granite Canyon (GC; Byrd, 1995), Leigh Lake (LL; Zellman et al., 2020b), and Steamboat Mountain (SM; DuRoss et al., 2020). Inset map shows the location of the study area in the US.

The correspondence in timing of the paleoseismic events at many of the individual trench sites suggests these earthquakes may have ruptured broad reaches of the fault, and potentially along its entirety (DuRoss et al., 2020). Such major scarp-forming events are considered to require earthquakes of magnitude Mw 7 (Smith et al., 1993; White et al., 2009; DuRoss et al., 2019).

In an effort to augment the direct evidence contained in trench exposures, sediments contained in glacially-scoured lake basins positioned along the Teton fault have been targeted to construct indirect inventories of past earthquake events. A continuous 14,000-year paleoseismic history constructed from multiple sediment cores recovered from Jenny Lake provides evidence for earthquake events on the central Teton fault at approximately 14.0 ka, 13.3 ka, 12.9 ka, 11.6 ka, 10.3 ka, 9.1 ka, 8.3 ka, 7.7 ka, and 5.3 ka (Larsen et al., 2019). The chronology of turbidites at Jenny Lake corresponds well to the ages of two large lake-terminating landslides, the timing of surface-rupturing earthquakes identified in the multiple trenches described above, and the preliminary chronologies of turbidite deposits identified in cores from four nearby lakes—Leigh, Bradley, Taggart, and Phelps Lakes (Figure 1; Blumm et al., 2019; Larsen et al., 2019). The presence of these additional lakes situated along the fault, combined with the multiple established trench datasets, presents high potential for constructing a remarkably detailed and robust paleoseismic history. It is therefore important to characterize the turbidite deposits at Jenny Lake to guide future analyses and to help improve the interpretation of paleoseismic records developed from additional Teton lakes and from similar lakes in other locations.

2.2 Jenny Lake

2.2.1 Lake and geomorphic system

Jenny Lake (43.76°N, 110.73°W; 2070 m asl) is located at the mouth of Cascade Canyon and occupies a terminal basin excavated by a major valley glacier during the Pinedale glaciation (Figures 1, 2). The lake is oval, with a surface area of approximately 5 km^2 (approximately 2.5 km x approximately 2 km), an average depth of 43 m, and a maximum depth of 73 m. Hydrologic input is dominated by seasonal snow melt derived from winter precipitation. Cold winters and thick snowpack result in prolonged lake ice cover, which commonly persists from December to May. Cascade Creek, which drains Cascade Canyon, is the primary sediment source to Jenny Lake. Sediments derived from erosional processes in the catchment are delivered to the lake by this stream, which has constructed an inflow delta along the western shoreline (Figure 2). Field observations confirm the delta surface is composed primarily of sub-angular to sub-rounded, fine to coarse sand and gravel. Lake outflow occurs to the south via Cottonwood Creek, a shallow overflow channel that transects a relatively subdued segment of the impounding terminal moraine complex (Figure 2). Mixed conifer forests are common at lower elevations in the catchment, including along Cascade Creek and on the inflow delta, moraine ridges, and hillslopes immediately surrounding the lake.
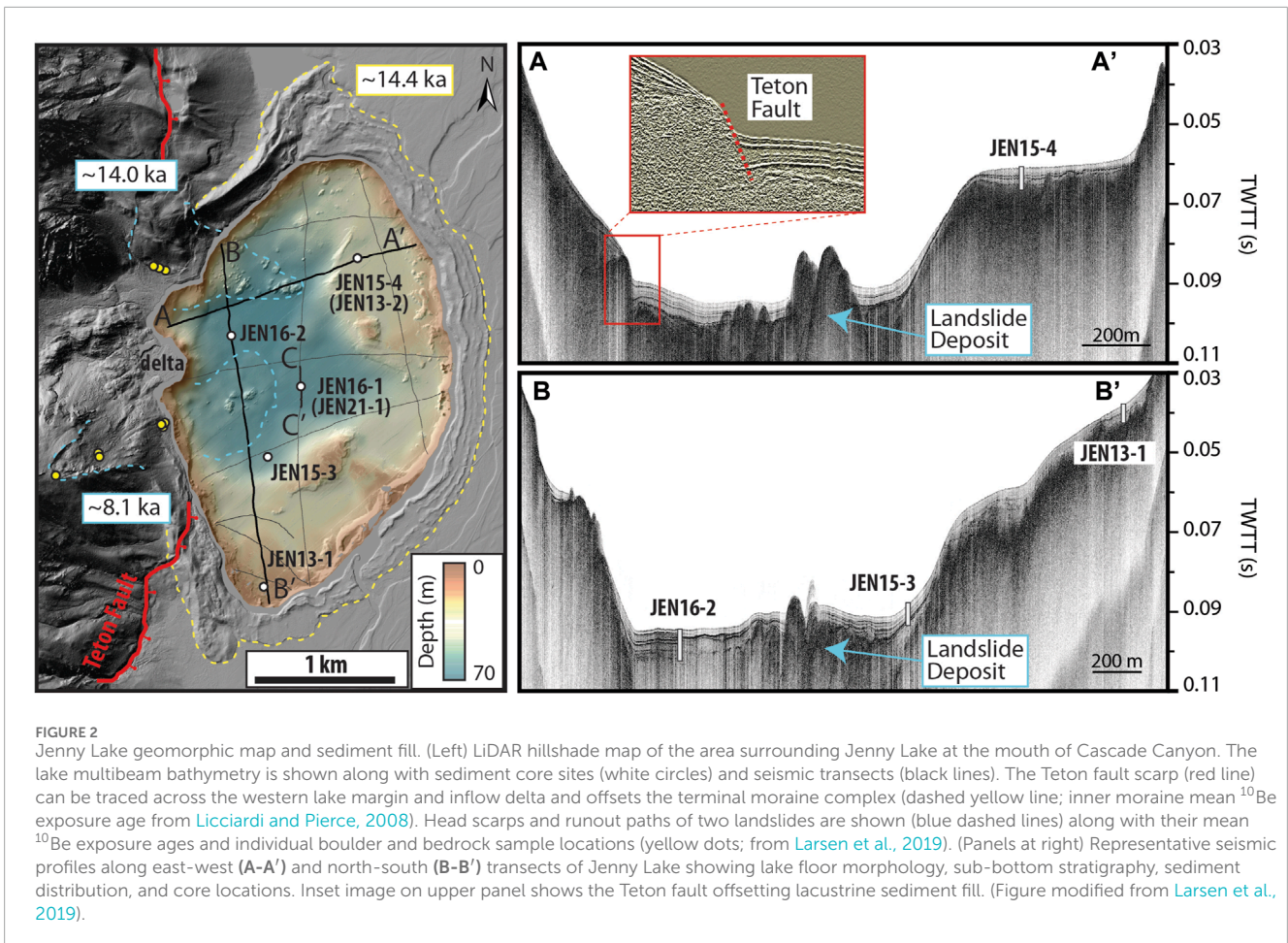
2.2.2 Lake sediment fill

Geophysical imagery (multibeam sonar and compressed high intensity radar pulse (CHIRP) sub-bottom profiling) reveal the lake bottom morphology and spatial distribution of lake sediment at high resolution (Figure 2; Larsen et al., 2016). The generalized bathymetry of Jenny Lake consists of a deep central basin in front of the canyon mouth that is surrounded by a broad outer shelf region (Figure 2). These two primary depositional settings contain well-stratified postglacial lacustrine sediments, ranging in thickness from <2.0 to approximately 8.5 m (Larsen et al., 2016; 2019). Along the western lakeshore, Lidar imagery captures the Teton fault trace as it cuts across the moraine deposits and under the lake. The submerged portion of the fault trace is captured by both multibeam and seismic imagery, which show it truncating the lake inflow delta and offsetting lake sediment fill (Figure 2; Larsen et al., 2019). Around the perimeter of the lake, the backslope of the terminal moraine continues steeply below the lake surface before intercepting the lakefloor. The mean exposure age of boulders deposited on the inner series of moraine crests is approximately 14.4 ka (Licciardi and Pierce, 2008; 2018). This date is supported by lowermost radiocarbon ages in lake sediment cores, indicating that Jenny Lake was formed prior to 14 ka and has been continuously accumulating sediment ever since (Larsen et al., 2019). The lake sediment fill is characterized as a succession of three main seismostratigraphic units, which reflect the evolution of the sedimentary system: a basal till unit that corresponds to glacial occupation of the lake basin, a laminated minerogenic unit that corresponds to the deglaciation of Cascade Canyon, and an upper low-density unit that corresponds to the nonglacial conditions of the past approximately 11.5 ka (Larsen et al., 2016). Interstratified within this stratigraphy are a series of earthquake-generated turbidite deposits (Larsen et al., 2019).

3 Methods

3.1 Lake coring and sediment properties

Sediment cores were collected from five locations in Jenny Lake in 2013, 2015, 2016, and 2021 using multiple types of piston coring systems deployed on cables from the frozen lake surface (Figure 2; Supplementary Table S1; for details of field and analytical methodology, see SI; Larsen et al., 2016; Larsen et al., 2019). The sediment sequence between all sites can be correlated using distinct changes in lithostratigraphy. This study focuses primarily on the Central Basin site (JEN16-1 and JEN21-1) (Figure 2). In 2016, one pair of offset and overlapped cores (JEN16-1A and JEN16-1B) were recovered from this location through repeated 2-m drives using a Uwitec coring system. Following collection, density and magnetic susceptibility were measured at continuous 5 mm intervals using Geotek core scanners at the National Lacustrine Core Facility (Laccore), University of Minnesota. In 2021, a third core (JEN21-1) was collected from this site using similar techniques to extend the composite record deeper into the sediment fill. The JEN16-1 and JEN21-1 cores were sub-sampled and analyzed for dry bulk density, total organic matter content (OM), and sand concentration. Total OM (weight % OM) was measured at continuous 2 cm intervals using loss on ignition (LOI) at 550°C for 4 h. To determine sand concentration (weight % sand grains >125 μm), 3 cm^3 of wet sediment was extracted from the cores using a volumetric sampler at continuous 5 cm intervals and at visible disturbance horizons. The sub-samples were transferred into beakers and submerged in

FIGURE 2
Jenny Lake geomorphic map and sediment fill. (Left) LiDAR hillshade map of the area surrounding Jenny Lake at the mouth of Cascade Canyon. The lake multibeam bathymetry is shown along with sediment core sites (white circles) and seismic transects (black lines). The Teton fault scarp (red line) can be traced across the western lake margin and inflow delta and offsets the terminal moraine complex (dashed yellow line; inner moraine mean [10]Be exposure age from Licciardi and Pierce, 2008). Head scarps and runout paths of two landslides are shown (blue dashed lines) along with their mean [10]Be exposure ages and individual boulder and bedrock sample locations (yellow dots; from Larsen et al., 2019). (Panels at right) Representative seismic profiles along east-west **(A-A′)** and north-south **(B-B′)** transects of Jenny Lake showing lake floor morphology, sub-bottom stratigraphy, sediment distribution, and core locations. Inset image on upper panel shows the Teton fault offsetting lacustrine sediment fill. (Figure modified from Larsen et al., 2019).

concentrated 30% hydrogen peroxide for 24–48 h to disaggregate the sediment and dissolve organic material before being washed and wet sieved through a 125 μm sieve and allowed to dry. The concentration of grain sizes >125 μm (fine sand) was determined by dividing the mass of the residual sediment by the initial sample volume.

3.2 Turbidite analyses

Turbidite deposits in Jenny Lake sediments were identified and described by Larsen et al. (2019) using visual observations and changes in sediment physical character. Here, we perform additional analyses of the six largest turbidites (those greater than 5 cm thick) common to all Central Basin (JEN61-1 and JEN21-1) cores to evaluate fine-scale changes in grain size distributions, mineralogical composition, and sedimentology. Grain size distributions through each turbidite deposit were measured at 5 mm intervals using a Malvern Mastersizer laser diffraction particle size analyzer coupled with a wet dispersion unit at the California State University at Fullerton and at Occidental College. At each interval, approximately 1 cm³ of sediment was extracted and pretreated to remove organic material using oxidation treatment through repeated baths in 30% hydrogen peroxide solution heated to 150°C. Once organic material was removed, samples were rinsed with distilled water and wet-transferred into beakers prior to being analyzed. An internal standard was run after every 10 samples to verify instrument

accuracy and repeatability (Fullerton standard: silica carbide powder (n = 96, median grain size = 13.1 μm, σ = 0.03 μm), Occidental standard: boron carbide powder (n = 54, median grain size = 12.2 μm, σ = 0.02 μm)). Statistical parameters of the grain size distributions, including skewness and geometric standard deviation (GSD; a measure of grain sorting) were calculated using the following equations:

$$GSD = \sigma = \frac{\sum X_i \left(d_i - \overline{d}\right)^2}{\sum X_i} \quad Skew = \frac{\sum X_i \left(d_i - \overline{d}\right)^3}{\sigma^3 \sum X_i}$$

where X_i = the number of particles in the ith size class, d_i = the median size of the ith size class, and $\overline{d}$ = the mean particle size.

Changes in elemental abundance through the turbidite deposits were determined at 2 mm resolution by scanning X-Ray Fluorescence (sXRF) using an Avaatech core scanner at the Scripps Institution of Oceanography, University of California at San Diego. XRF measurements were made at voltages of 10 kV using an exposure time of 10 s and current of 500 mA (Addison et al., 2013). We performed a Principal Component Analysis (PCA) that incorporated sediment grain size metrics (D50, sand %, clay %, silt %, geometric standard deviation (GSD), and skew), elemental abundance (K, Si, Al, Ti, Fe, Ca), density, and magnetic susceptibility data for each turbidite event using the PCA function within the R package FactoMineR with default settings (Lê et al., 2008; see SI text). To directly compare variations of the different data through

each deposit, all properties were placed on a common depth scale of 2 mm-intervals by interpolating the MS and grain size data using the approx function in R. This function eliminates the possibility of introducing bias into the PCA by not including missing values.

The ages of individual turbidites at Jenny Lake were first determined by Larsen et al. (2019) by dating material deposited within 200 years of the top and/or bottom contact of each deposit. Here, we improve the age control at the JEN16-1 site by adding six additional radiocarbon ages and transfer the updated chronology to the new JEN21-1 core (for additional geochronological information and methods, see SI text, Supplementary Figure S5; Supplementary Tables S2, S3).

4 Results

4.1 Sediment core stratigraphy

Sediment cores recovered from Jenny Lake range in length and approximate basal age (Supplementary Table S1). Cores collected from sites in the deep central basin (JEN16-1 and JEN21-1) and outer shelf (JEN15-4 and JEN13-2) penetrate down to strongly laminated sediments containing ice-rafted debris (IRD), indicating nearly complete recovery of the postglacial interval (Figure 3). These cores reveal a coherent two-component lithostratigraphic sequence of clay-rich, laminated or massive light gray to gray glacial-lacustrine sediments overlain by an upper unit of mostly homogenous or faintly laminated olive brown to brown non-glacial sediments (Figure 3; see Supplementary Figures S1–S4 for individual core images). A gradational contact separates these two sediment packages and reflects the decreasing influence of glacial erosion on lake sedimentation and shift toward non-glacial conditions at the end of the Pleistocene. The depth to this transition and other stratigraphic markers increases with water depth and proximity to the inflow delta, confirming that sediment accumulation rates in the central basin are greater than the surrounding shelf and that Cascade Canyon has been the dominant source of sediment to the lake.

Interstratified within the general lithostratigraphic sequence are two prominent rhyolitic air-fall tephra layers and a series of other event deposits (Figure 3). The tephra layers have been geochemically characterized and assigned to the Mazama (7.6 ka; Egan et al., 2015) and Glacier Peak (13.6 ka; Kuehn et al., 2009) ash beds (Larsen et al., 2016). These tephra layers aid in the stratigraphic correlation between cores taken throughout the lake. The other event deposits range in thickness, sedimentary texture, and frequency. At site JEN16-2, proximal to the inflow delta, the upper sediment sequence contains numerous sand layers ranging in thickness from 1 to 10 cm and composed predominantly of fine to coarse sand grains with abundant woody terrestrial plant material (Figure 3; Supplementary Figure S2). The layers do not present consistent sedimentary structure or grading but tend to have a moderately sharp basal contact of coarse sand and a more diffuse upper contact where organic material (e.g., twigs, conifer needles, cone fragments, etc.) contained in a sandy matrix grade into the overlying host sediments. Apart from these qualities, the organic-rich sand deposits do not show a strong stratigraphic pattern and are absent in cores from other sites, indicating these chaotic deposits are spatially restricted to the region near the inflow delta.

In addition to the sand layers at JEN16-2, all core sites contain well-defined, normally-graded turbidite deposits (Figure 3). These deposits range in thickness and are easily correlated between sites around the lake based on their characteristic stratigraphic expression and the individual chronologies respective to each core. The relative thickness of individual turbidite deposits is greatest in the central basin and at site JEN16-2, where they are up to 48-cm-thick (Figure 3). The cores taken from the distal eastern and southern regions of the outer shelf contain fewer turbidites and they are relatively thin compared to their correlative deposits in the central basin. One exception to this trend is the thick turbidite (39-cm-thick) present in the glacial unit at JEN15-4 (Figure 3).
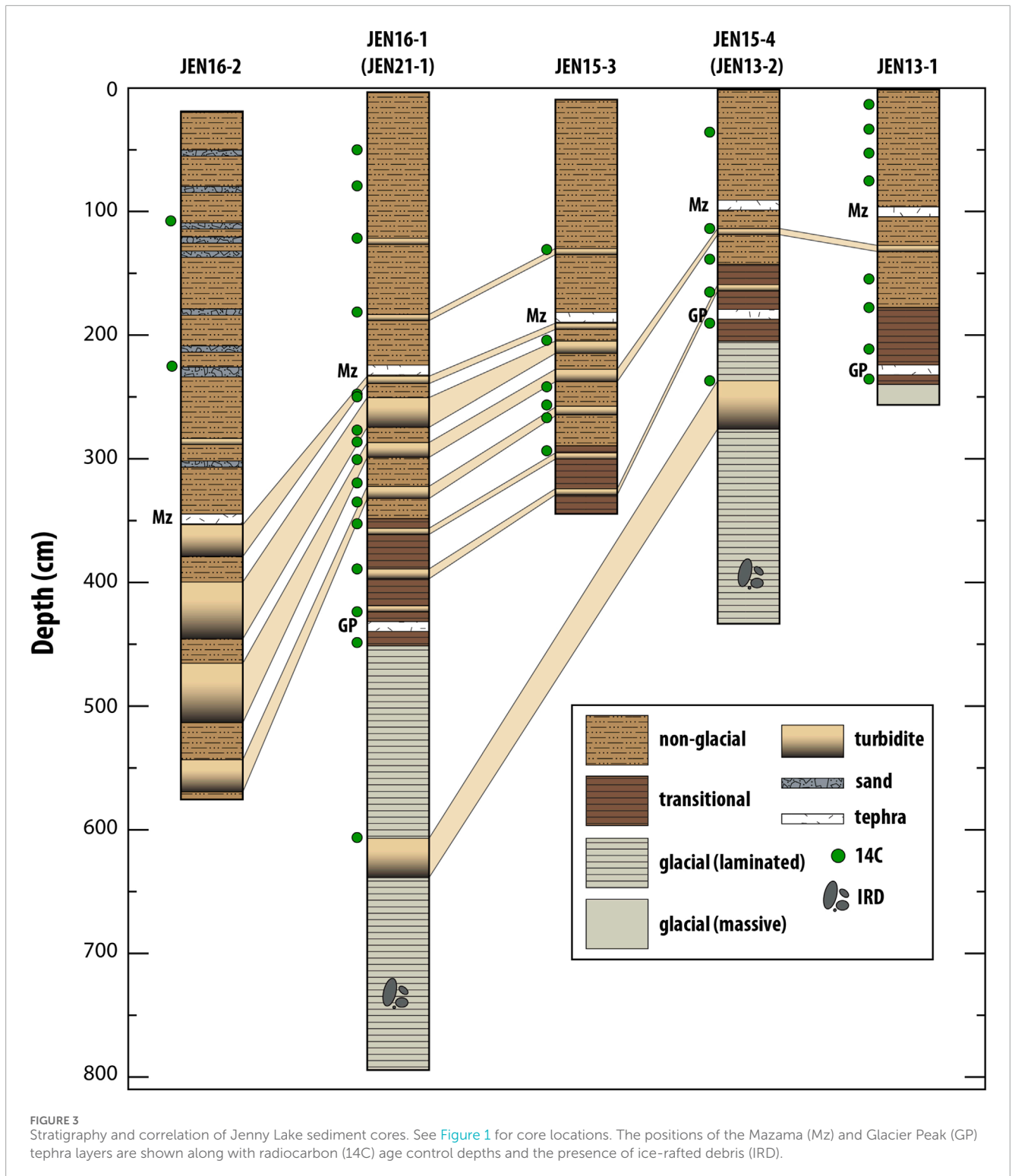
4.2 Sediment properties

Average sediment density values and OM concentrations at the Central Basin site are 1.6 ± 0.3 g/cm^3 (range: 1.1–2.2 g/cm^3; n = 2097) and 6.1% ± 3.8% (range: 0.5%–17.5%; n = 843), respectively (Figure 4). The concentration of siliciclastic sand (grains >125 μm) ranges from 0 to 1.5 g/cm^3 (n = 304). A long-term pattern of decreasing density and increasing organic content toward the core top tracks changes in seismic stratigraphy and core lithostratigraphy (Figure 4). In general, the glacial unit is characterized by dense, minerogenic sediments deposited during the overall phase of deglaciation. The lithologic transition from glacially influenced sedimentation to non-glacial sedimentation that occurs near the start of the Holocene reflects catchment stabilization and reduced minerogenic sediment flux (Larsen et al., 2016).

The most notable features of the Jenny Lake sediment record are the rapid changes in density, sand content, and organic matter associated with the series of turbidites (Figure 4). These deposits are identified in core section by recognizable changes in sediment texture. In seismic imagery, the turbidites are expressed as a series of high-amplitude seismic reflectors that can be traced around the basin (Figure 4; Larsen et al., 2019). Abrupt increases in sand and density and a decrease in organic content occur at the base of each turbidite. For most of the events, sediment density increases from background values of approximately 1.4 g/cm^3 to maximum values of approximately 2.0 g/cm^3. Density values generally remain higher than background through the entirety of each deposit. Similarly, sediment OM concentration decreases from background values at the base of each turbidite, remains low through the deposits, and immediately returns to background values in overlying sediments (Figure 4). One exception to this trend in OM content is the thick event deposit at approximately 2.6 m depth, which contains a brief peak in OM that is associated with interstitial woody plant remains visible in core section (Figure 4). Outside of the defined spikes in sand and density associated with the turbidite deposits, sediments at this site in the central basin contain negligible sand content and background sedimentation during the non-glacial interval is dominated by deep-water hemipelagic silts (Figure 4).
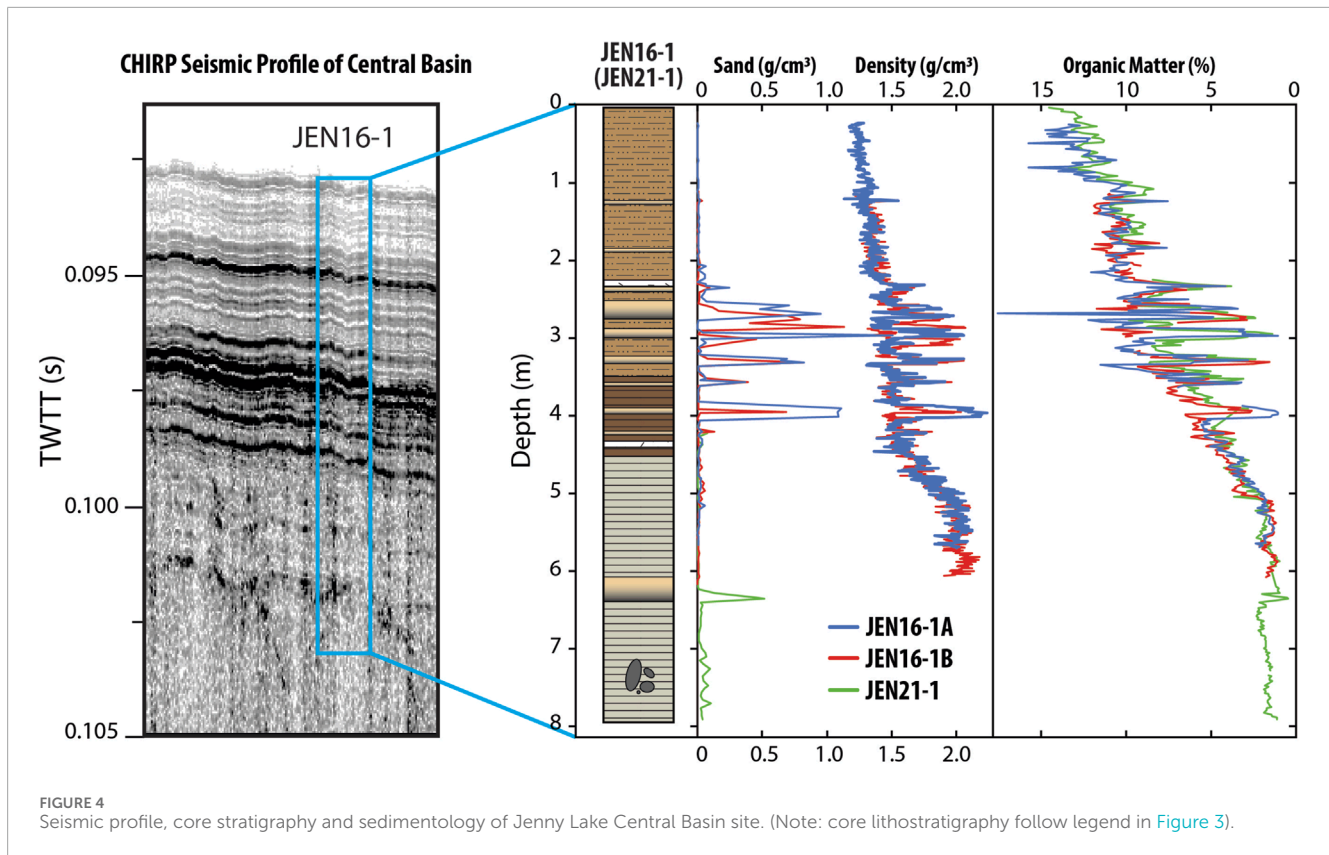
4.3 Turbidite stratigraphy

The six most prominent turbidite deposits at the Central Basin site (JEN16-1 and JEN21-1) have thicknesses of approximately

FIGURE 3
Stratigraphy and correlation of Jenny Lake sediment cores. See Figure 1 for core locations. The positions of the Mazama (Mz) and Glacier Peak (GP) tephra layers are shown along with radiocarbon (14C) age control depths and the presence of ice-rafted debris (IRD).

34 cm, 8 cm, 12 cm, 12 cm, 24 cm, and 6 cm, and occurred at 13.9 ± 0.6 ka, 12.9 ± 0.1 ka, 10.3 ± 0.2 ka, 9.1 ± 0.1 ka, 8.4 ± 0.1 ka, 7.7 ± 0.1 ka, respectively (uncertainty reported as ± 2 SD) (Figure 5, Supplementary Tables S1, S3). We note that, despite the addition of six new radiocarbon ages, the calculated age and uncertainties for these deposits are statistically identical to those previously reported by Larsen et al. (2019), with only nominal differences. For clarity,

we apply these turbidite ages when referring to the individual event deposits (Figure 5).

In all cases, the top and bottom contacts of the event deposits are sharp and clearly defined from background sediments by changes in textural properties and grain size distributions (Figure 6). Changes in the fractional abundance of grain sizes and median grain size (D_{50}) also define a stratigraphic pattern within each event deposit

Seismic profile, core stratigraphy and sedimentology of Jenny Lake Central Basin site. (Note: core lithostratigraphy follow legend in Figure 3).

composed of 1) a thick coarse-grained basal unit of mostly sand, 2) a middle unit of mostly silt and very fine sand, and 3) a comparatively thin, fine-grained cap unit made of very fine to fine silt and clay (Figure 6). The boundaries between successive units are relatively sharp indicating strong segregation of particle sizes during discrete phases of deposition. The coarse basal sand unit is relatively well-sorted and contains D_{50} values between approximately 85 μm and approximately 265 μm, depending on the deposit (Figure 6). In comparison, the D_{50} in background lake sediments is generally between 15 and 25 μm (Figure 6). Above the sand unit, D_{50} and grain sorting decrease step-wise into the middle silt unit and again into the upper clay unit, with the finest grain sizes (D_{50} values of 2.5–15 μm) and poorest sorting comprising the clay-rich cap layer (Figure 6).

Principal Component Analysis (PCA) can be performed in stratigraphic assessments to characterize and statistically differentiate units (e.g., Praet et al., 2020). Here, the PCA results show broadly consistent associations between elemental abundance, grain size, and other sediment parameters across all events (Figure 7). The primary principal component (PC1) captures between 53.95% and 77.19% of multivariate variability and is predominantly controlled by sediment grain size with positive and negative PC1 values corresponding to fine and coarse grain sizes, respectively. The second principal component (PC2) captures between 10.98% and 26.95% of multivariate variability and appears to be influenced by secondary elemental relationships. A common feature of the PCA is the clustering of sand content, D_{50}, and density in negative PC1 space while clay content and silt content generally plot together near positive PC1 (Figure 7). The elemental data relationships are less consistent. Elemental abundance generally aligns with positive PC1, suggesting a greater abundance of these elements in clay- and silt-sized particles, which tend to cluster closest to positive PC1 and near magnetic susceptibility. Geometric standard deviation (GSD) and skewness plot consistently between positive PC1 and negative PC2 (Figure 7).

The PCA results also highlight a consistent relationship between stratigraphic depth within the event deposits and variations in the sedimentary parameters captured by PC1 and PC2. The basal (coarse-grained) and upper (fine-grained) portions of the events are consistently dominated by PC1 while mid-depths show variable associations with PC2 (Figure 7). This relationship indicates that sedimentary characteristics of the basal unit and top unit are best correlated with PC1, with a minimal but variable contribution of positive and negative PC2, while those at intermediate depths show decreasing association PC1 and an increasing association with PC2 (Figure 7).

5 Discussion

5.1 Earthquake-generated turbidites in Teton lakes

The geomorphologic and tectonic setting of the range-front Teton lakes make them particularly well-suited to record seismic activity. Moreover, the lake records are continuous and can be established with high chronological resolution, providing an ideal complement to the nearby paleoseismic trench exposures. Steep subaqueous slopes and relatively high rates of sediment
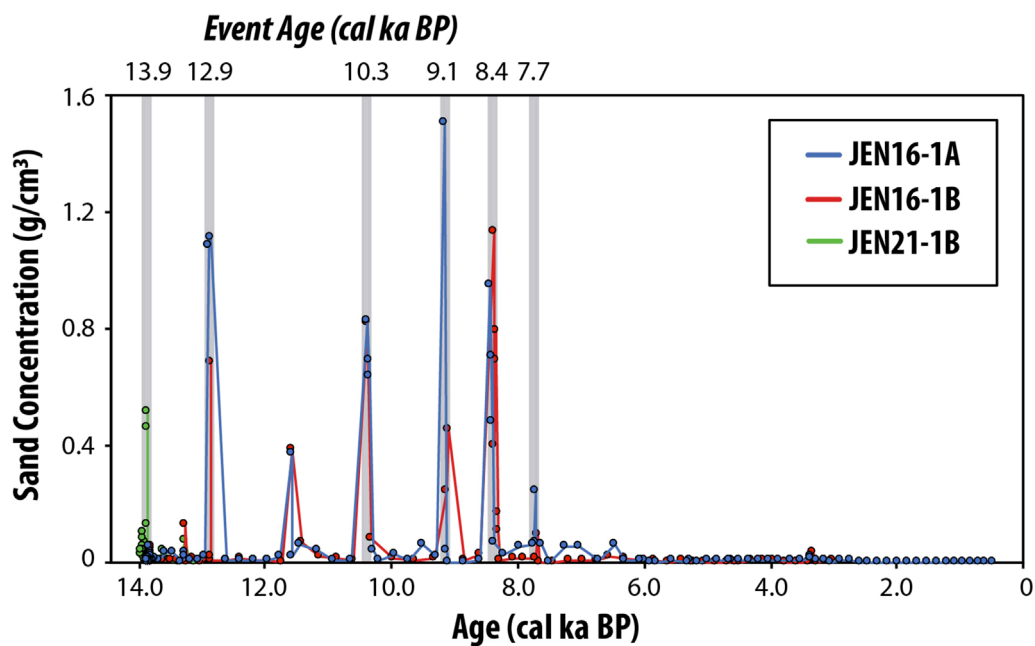
FIGURE 5
Time series of sand concentration (grains >125 μm) measured in sediment cores collected from the Central Basin site (JEN16-1/JEN21-1). The ages of the six thickest turbidite deposits and inferred earthquake events are highlighted with grey bars.

delivery to the lakes results in the replenishment of lacustrine and deltaic sediment supply available for successive earthquake-triggered failures and provides ample stratigraphic spacing of individual turbidite deposits in core section—thus aiding in their identification and ability to be accurately dated.
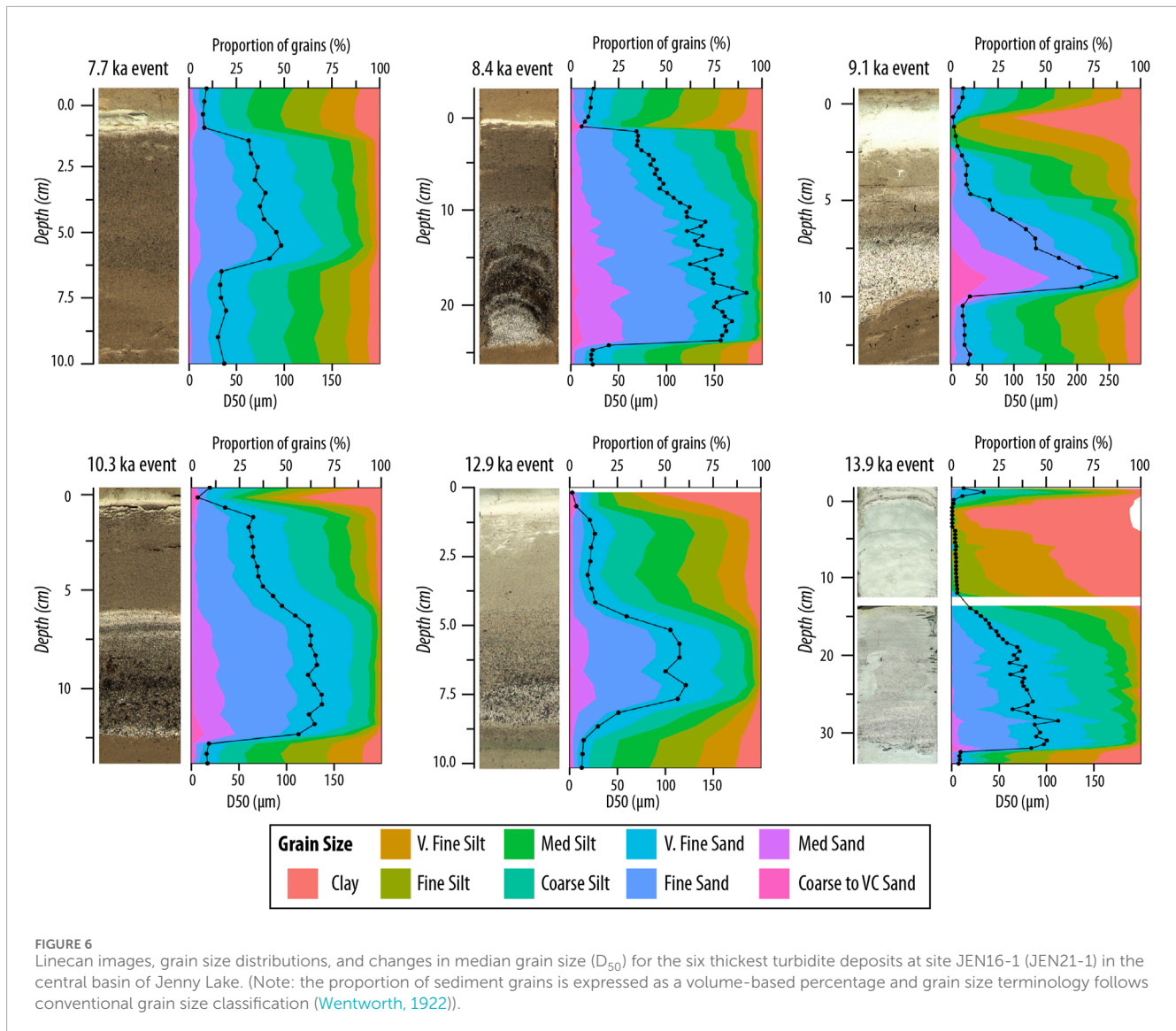
We suggest that the characterization of earthquake-generated turbidites at Jenny Lake provides a model for their formation in this setting and establishes a framework for identifying, characterizing, and correlating earthquake-generated deposits in nearby basins. Similar piedmont lakes (Phelps, Taggart, Bradley, and Leigh) span a broad section of the fault and together, present a rare opportunity to develop multiple cross-evaluated, temporally-long (14 ka), and detailed earthquake records (Figure 1). In the following discussion, we present the Jenny Lake sediment record in the context of improving the postglacial paleoseismic history of the Teton fault with an emphasis on coseismic sedimentary processes in and around the piedmont lakes.

5.2 Stratigraphy of seismic events at Jenny Lake

The generalized stratigraphy of Jenny Lake turbidites is consistent and begins with a sharp basal contact with underlying sediments followed by a well-defined sedimentary sequence (Figure 6). Based on patterns in grain size distributions and in accordance with descriptions of coseismic turbidite stratigraphy observed in similar lake settings (e.g., Beck, 2009), we categorize the turbidites into three primary components—a basal coarse sand unit, a middle silt unit, and an upper clay-rich cap. These sub-divisions are clearly differentiated by changes in grain sizes, which suggest a

step-wise decrease in the energy of the depositional environment during the overall phase of deposition (e.g., Bertrand et al., 2008) (Figure 6). Distinctive relationships between textural and geochemical properties of each component are highlighted for the 10.3 ka turbidite event (Figure 8). The sand unit ("Unit I") is relatively thick, has a sharp erosive basal contact, maximum grain size values, and high density (Figure 8). The properties of this unit are indicative of deposition by a relatively high-velocity current. For most events, it is well-sorted and reveals either mostly massive grading or a slight fining-upward pattern. One exception to this trend is the sand unit in the 9.1 ka event, which contains a strong fining-upward pattern (Figure 6).

We suggest the coarse sediments associated with the sand unit are sourced primarily from the steep subaqueous slopes around the lake perimeter, and particularly from the inflow delta. Steep slopes are an important characteristic of Teton lakes with regard to sediment transport mechanisms. Slope failures at Jenny Lake are revealed by bathymetric imagery, which shows numerous sediment piles at the base of the moraine along the lake's perimeter and landslide deposits (Figure 2; Larsen et al., 2019). On their western shores, the Teton fault runs along hillslopes at the mouths of the respective glacial valleys and directly across the lake inflow deltas (Figure 1). The Gilbert-style deltas are composed of relatively coarse sediments with a steeply-dipping foreslope that descends to the central deep basin of each lake. Seismic imagery and core stratigraphy at Jenny Lake confirm that sediment transport to the lakes occurs primarily through the inflow delta system. We suggest that high slope angles and the continuous supply of sediment sourced from the catchment render the submerged delta fronts unstable and vulnerable to failure, including in response to strong ground shaking during earthquakes. In such settings, delta slope

FIGURE 6
Linecan images, grain size distributions, and changes in median grain size (D_{50}) for the six thickest turbidite deposits at site JEN16-1 (JEN21-1) in the central basin of Jenny Lake. (Note: the proportion of sediment grains is expressed as a volume-based percentage and grain size terminology follows conventional grain size classification (Wentworth, 1922)).
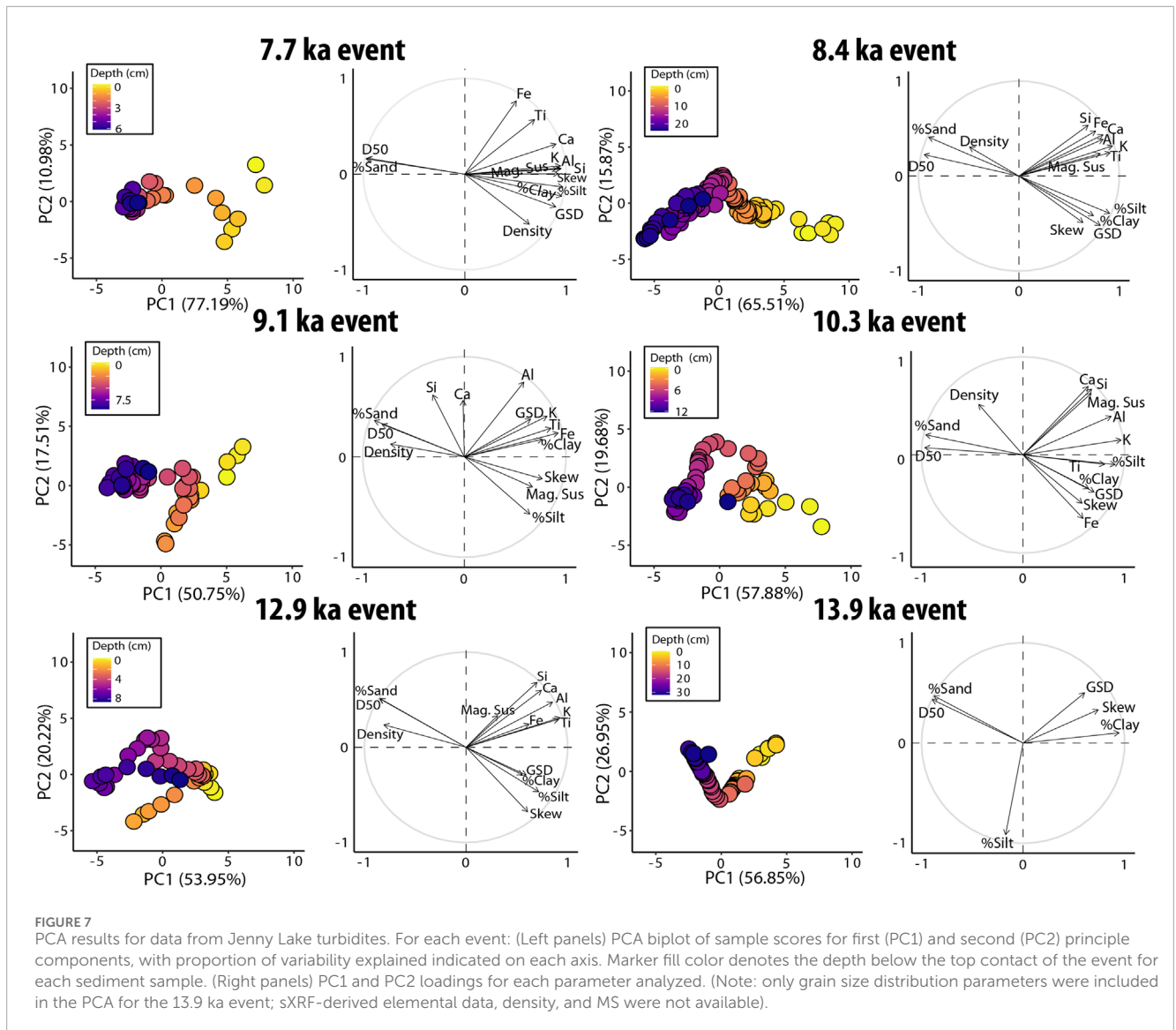
failures that result in a mass flow can result in diagnostic turbidite deposits in the basin (Beck, 2009; Sabatier et al., 2022). Due to the hypsometry of the Teton lake basins and their position along the range front, delta failure and/or destabilization of other subaqueous slopes would generate a high-density flow and the immediate delivery and focusing of coarse sediments to the lake's central basin.

The next stratigraphic component is the silt unit ("Unit II") (Figure 8). It is relatively thick, composed of fine silts to very fine sands, and reveals either massive grading or a modest fining-upward pattern, depending on the deposit (Figure 6). The boundary between the underlying sand unit and this unit is relatively well-marked by changes in grain size and other parameters, including a slight decrease in grain sorting and density and increased K, Ti, and Fe content (Figure 8). The finer texture of this unit reflects a reduction in the energy of the depositional environment. In some settings, co-seismic turbidites contain a layer of reworked terrestrial organic material interstitial to the sand and/or silt units (e.g., Bertrand et al., 2008). At Jenny Lake, the only turbidite that contains appreciable organic material is the 8.4 ka event (Figure 6). As discussed below,

this particular turbidite is associated with a contemporaneous lake-terminating landslide event, which we suggest may have contributed terrestrial plant material to the deposit.

The clay-rich cap is the top unit ("Unit III") of the turbidite sequence and expressed as a relatively thin layer of clay to fine silts (Figure 6). The clay cap is characterized by relatively poor sorting and modestly increased density and Fe and K content (Figure 5). We suggest the notable decrease in grain sorting of this unit may reflect the contribution of coarser grains due to the resumption of background sedimentation. The very fine-grained sediment in this layer is likely sourced from previously deposited lake sediments, including the glacial lithostratigraphic unit. We suggest previously-deposited clays and fine silts are mobilized during strong ground shaking, resuspended in the water column, and redistributed throughout the lake due to turbidity currents and seiching, with the finest particles settling last (i.e., during the ice-covered season when the absence of wave energy enables the settling of fine grains). A seiche wave -triggered by coseismic subaqueous slope failures, subaqueous fault displacement, and/or
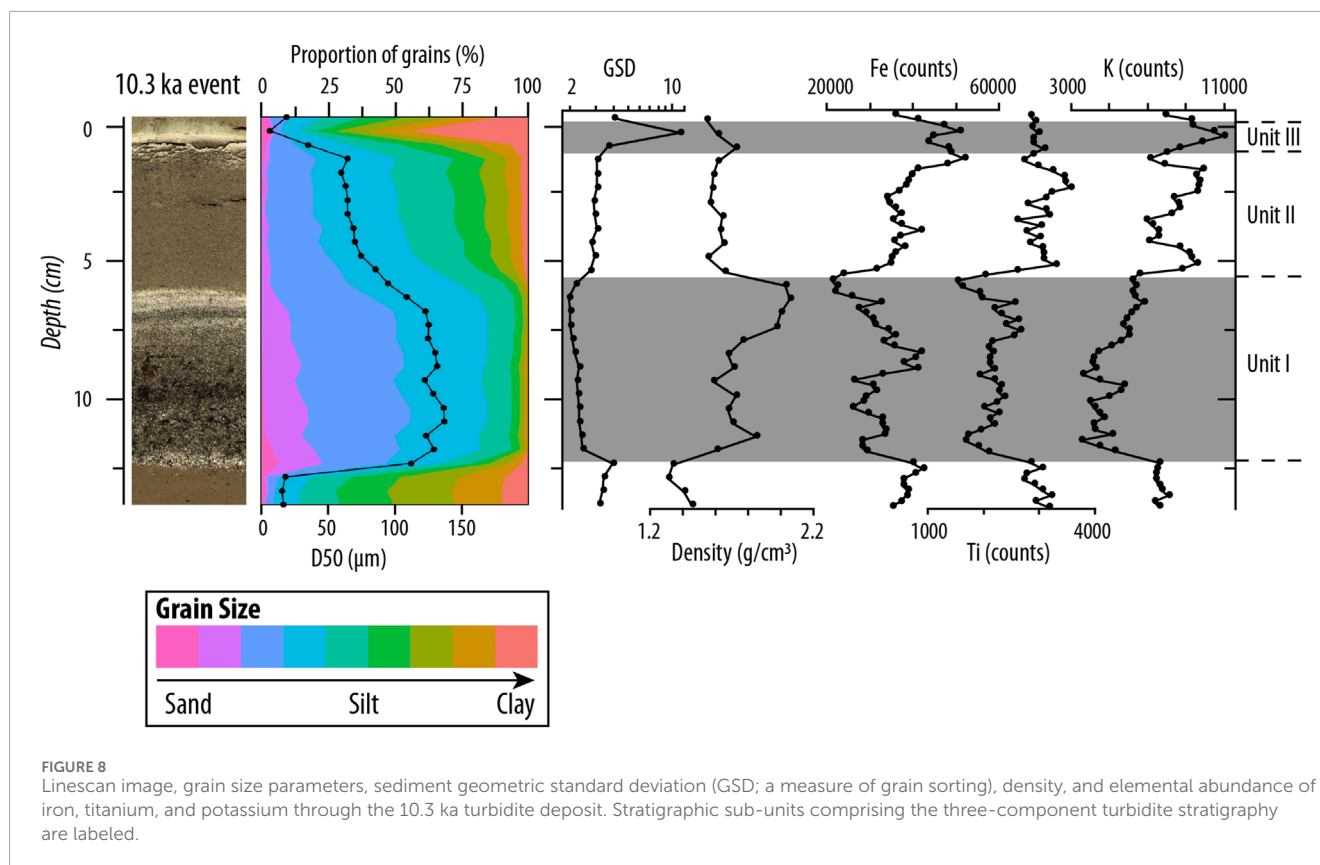
FIGURE 7
PCA results for data from Jenny Lake turbidites. For each event: (Left panels) PCA biplot of sample scores for first (PC1) and second (PC2) principle components, with proportion of variability explained indicated on each axis. Marker fill color denotes the depth below the top contact of the event for each sediment sample. (Right panels) PC1 and PC2 loadings for each parameter analyzed. (Note: only grain size distribution parameters were included in the PCA for the 13.9 ka event; sXRF-derived elemental data, density, and MS were not available).

landsliding into the lake-would act to remobilize additional clastic material from near-shore regions and/or trigger backslope failures of the impounding moraine. Seiching may have also contributed to the observed focusing of the deposit in the central basin and increased segregation between fine- and coarser-grained particles, which resulted in the distinct 3-component stratigraphy (e.g., Bertrand et al., 2008; Beck, 2009).

5.3 Differentiating earthquakes and floods

Given their potential to exhibit similar features, differentiating between flood and earthquake-generated turbidites remains an important objective of investigations into event deposits in lake sediments (e.g., Praet et al., 2020; Vandekerkhove et al., 2020; Sabatier et al., 2022). Some studies benefit from the identification and characterization of individual turbidites that were generated by documented historical events (St-Onge et al., 2004; Beck, 2009; Daxer et al., 2022; Fan et al., 2023). However, without an historical

flood or earthquake event to use as a sedimentary fingerprint, differentiation between these two triggers is primarily based on recognition of distinctive sedimentological characteristics and basin-scale distribution patterns associated with inferred sedimentary processes (e.g., Beck, 2009; Praet et al., 2020; Vandekerkhove et al., 2020). For example, differences between the quasi-stable *versus* quasi-instantaneous flow and depositional style associated with flood and earthquake-derived deposits, respectively, can help in attributing a trigger mechanism. Strong ground shaking during an earthquake is expected to induce subaqueous slope failure and a short period of high hyperpycnal flow that gradually wanes (Mulder and Alexander, 2001). Previous studies demonstrate that shaking-induced delta collapse and/or failures of other subaqueous slopes result in a sharp basal contact and a relatively coarse sand unit (e.g., Bertrand et al., 2008). In contrast, the hyperpycnal flow induced by floods typically lasts longer and is somewhat steadier in flow velocity (Alexander and Mulder, 2002; Mulder et al., 2003). Additionally, flood water is more likely to "bypass" the coarse sediments of the delta front, which results in a comparatively

FIGURE 8
Linescan image, grain size parameters, sediment geometric standard deviation (GSD; a measure of grain sorting), density, and elemental abundance of iron, titanium, and potassium through the 10.3 ka turbidite deposit. Stratigraphic sub-units comprising the three-component turbidite stratigraphy are labeled.

fine-grained deposit that commonly lacks an erosive basal contact (Mulder and Alexander, 2001; Beck, 2009). Some studies of flood deposits in lake sediments observe a distinctive two-unit structure consisting of a silt and clay layer (Mulder and Chapron, 2011). While earthquake deposits are expected to show variable distribution and thickness within the basin (Vandekerkhove et al., 2020), the hyperpycnal flow during a flood event carries sediment across the basin, resulting in a more-even basin-wide spatial distribution and thickness from mixing and settling evenly throughout the lake (Praet et al., 2020; Vandekerkhove et al., 2020).

The stratigraphical and statistical (PCA) similarity of turbidite deposits at Jenny Lake suggests a common trigger mechanism (Figures 6, 7). We infer the trigger to be earthquake activity along the Teton Fault, which is evidenced by the distinct three-component stratigraphy and strong basal contact of the turbidites, their spatial distribution and variable thickness, and their temporal agreement with trench investigations. We would expect flood-generated deposits in Teton lakes to be comparatively fine-grained, lack an erosive basal contact or strong three-component stratigraphy, and display a more-uniform distribution throughout the basin. However, we acknowledge the degree of similarity between flood and earthquake-generated deposits are highly contingent on the local geomorphic system (e.g., Sabatier, 2022) and that a universal expression across all Teton Lakes cannot be assumed. We therefore suggest careful correlation and analysis of a multi-lake record may aid in improving our understanding of the nuanced relationship between basin morphology and the stratigraphic expression of co-seismic turbidites.

5.4 Co-seismic landslides and their impact on turbidite stratigraphy

Hillslopes in and around the Teton Range are susceptible to landslides (e.g., Love et al., 1992; Crosby, 2019; Johnson et al., 2022). Here, we refer to landslides broadly as incorporating a range of mass movement events that describe flows, slides, and falls of earth materials. Evidence of past landslides can be observed on the steep canyon walls in the interior of the mountain range and along the eastern range front, where in places, they transect the Teton fault scarp and/or run out into lake basins (Crosby, 2019; Zellman et al., 2019). For example, the floor and walls of Cascade Canyon are blanketed by colluvium, talus, and alluvial fan deposits that have accumulated since deglaciation approximately 15 ka. Landslides occurring over this timescale have affected large portions of the Canyon and are considered to be important agents of clastic sediment production and transport (e.g., Tranel et al., 2015; Johnson et al., 2022).

Above the western shore of Jenny Lake, prominent landslide scars are visible in the hillslopes adjacent to the fault trace (Figure 2). One landslide south of Cascade Canyon originated on a steep bedrock slope in Late Archean crystalline rocks, and another originated in poorly consolidated moraine deposits and colluvium to the north (Love et al., 1992; Figure 2). The runout paths of both features can be mapped into the lake's central basin where they terminate as block and fan deposits visible in bathymetric and seismic imagery. High-amplitude seismic reflectors extending laterally from these deposits indicate

the two events were coincident with and/or contributed to widespread deposition of a layer of anomalously dense sediments around the lake.

Larsen et al. (2019) dated the two landslides above Jenny Lake using [10]Be inventories of boulder and bedrock surfaces, which yielded mean ages of approximately 8.1 ka and approximately 14.0 ka for the two landslides, respectively (Figure 2). The landslides ages are coincident with two radiocarbon-dated turbidites in the Jenny Lake sediment sequence and preliminary ages of two turbidites identified in nearby lakes Bradley and Taggart (Blumm et al., 2019; Figure 1). Both of these turbidites are remarkably thick at the Central Basin core site (24-cm-thick and 34-cm-thick, respectively) but otherwise present a similar stratigraphic expression to other turbidites at Jenny Lake, suggesting a similar process of formation. The earlier event is also fully expressed in core JEN15-4 recovered from the distal eastern portion of the lake, on a shelf approximately 23 m above the central basin (Figures 2, 3). At this site, the coarse basal unit of the 13.9 ka turbidite contains rounded clasts of gneiss and quartzite cobbles, up to 8 cm in diameter, that were likely sourced from the backslope of the terminal moraine due to seiching (Larsen et al., 2019). There is no lithologic source of quartzite cobbles in Cascade Canyon but they are a common component of the terminal moraine complex, which was developed in part by the buildup of quartzite-rich outwash sourced from regions to the north of Jackson Hole during the Pinedale glaciation (Pierce and Good, 1992). The younger 8.4 ka turbidite deposit is contained in the Central Basin cores and at other core sites. In contrast to all other turbidites, this deposit is notable for an unusually high amount of interstitial woody plant remains that are clearly visible in core section and register as increased OM and decreased density values (Figures 3, 4). We suggest the woody plant material incorporated in this deposit was delivered to the lake directly by the landslide and by seiching, which could have remobilized OM from nearshore regions and focused it in the central basin. We further speculate that the lack of organic matter contained in the older 13.9 ka turbidite is a function of the age of this deposit, which occurred soon after ice retreat from the lake basin when the hillslopes around the lake, and particularly the freshly deposited moraines, may have supported only minimal woody vegetation.

The available evidence strongly suggests that the two lake-terminating landslides at Jenny Lake occurred coincident with the timing of earthquake events and contributed clastic material and organic remains to the resulting turbidite deposits. We note that past landslides throughout the Tetons were most likely driven by both seismic and aseismic factors (e.g., glacial over-steepening, extreme precipitation events, wildfires, etc.). However, we demonstrate that in some cases, deep-seated landslides in the Tetons may have been triggered by major earthquake events. The potential for strong earthquakes to trigger slope failures presents significant hazards to visitors of Grand Teton National Park and to local infrastructure, yet an incomplete record of both postglacial seismicity and landsliding impedes our ability to characterize the relationship and magnitude of these coupled hazards. We suggest future work combining paleoseismic histories with efforts to construct landslide inventories and chronologies could help elucidate patterns of past seismically-induced landslide activity in the Tetons.

5.5 Controls on turbidite properties

The relationship between local seismic intensity and turbidite properties (thickness, grain size) has been explored in various lake settings around the world (e.g., Beattie and Dade, 1996; Van Daele et al., 2015; Daxer et al., 2022) and some studies have quantitatively estimated paleomagnitude using such relationships (e.g., Hibsch et al., 1997; Rodriguez-Pascua et al., 2003; Moernaut et al., 2014; Van Daele et al., 2015; Daxer et al., 2022). It is intuitive that stronger ground shaking can mobilize greater sediment volumes and result in thicker turbidites (e.g., Goldfinger et al., 2012; Moernaut et al., 2017), and that ruptures resulting in delta failure can yield especially coarse deposits in proximal basins (e.g., Beck, 2009). However, despite these first-order controls, the nuanced relationship between turbidite character and paleoearthquake magnitude are likely to be site-specific and influenced by numerous additional factors. For example, coseismic turbidite properties (thickness, grain size distributions, sharpness of basal contact) are largely controlled by the interaction of basin morphology with the many tectonic, climatic, and geomorphic processes that influence local sediment supply across a range of timescales (e.g., production, transport, and deposition of sediment in and around the lake) (e.g., Bouma, 2004; Howarth et al., 2012; Wilhelm et al., 2016; Praet et al., 2020). Increased sediment supply maximizes the amount of sediment available to be mobilized during slope failure and therefore maximizes potential turbidite thickness. Basin morphometry can influence turbidite thickness as the size, shape, and proximity to the sediment source influence the volume of sediment delivered to any particular location in the basin. Similarly, changes in climate can influence turbidite properties by governing the production, transport, and character of sediment through the catchment over a variety of timescales. Sediment supply is also influenced by other factors such as the time elapsed since the last earthquake event and/or the recurrence intervals of other disturbance events that control sediment flux (e.g., glaciations, floods, wildfires, landslides, etc.).

These factors discussed above, and many others highlight the importance of varying sediment supply when relating turbidite properties at a given core site to seismic intensity. As stated earlier, we suggest the Teton lake inflow deltas are a key source of sediment remobilized during earthquake events. We further suggest that delta failure and other slope failures are not constrained by sediment influx. This is demonstrated by the relatively high accumulation rates and potentially by the repeated sand units in the upper sequence of JEN16-2 (Figure 2). The chaotic sand units occur during a prolonged interval of inferred seismic quiescence and are only present proximal to the delta front (Figures 2, 3). We speculate that these chaotic deposits reflect episodes of minor delta failure at Jenny Lake during times when the inflow delta is not periodically reset by seismic shaking and thus susceptible to slope instabilities triggered by aseismic factors (e.g., sediment overload, storms, etc.). Therefore, assuming delta failure is not limited by sediment influx, we deduce a first-order relationship between turbidite properties and the degree of ground shaking. This potential relationship may be strengthened by comparison to other proximal lake basins. A similar approach was followed by Moernaut et al. (2014), who used the composite turbidite

thickness across multiple lake basins to estimate the paleomagnitude of megathrust events in Chile. Additionally, a comparison of the thickness of synchronously deposited events across lake basins may aid in determining local seismic intensity, epicenter location and/or rupture length. Thus, while we acknowledge that turbidite thickness at any single location within a lake may be partly influenced by earthquake magnitude, we suggest that the stratigraphic expression and presence of synchronous turbidite deposits in multiple lake basins positioned along fault strike may be a more meaningful indicator. Future work that develops and correlates additional paleoseismic records across multiple range-front Teton lakes and trench datasets may provide a framework for understanding and interpreting the intricate relationship between turbidite properties and seismic intensity.

6 Conclusion and future work

The range-front Teton lakes are well-suited to record seismic activity of the Teton normal fault since their formation approximately 15,000-years ago. Past earthquake events that generated slope failures in and around Jenny Lake are expressed stratigraphically as a series of coseismic turbidite deposits, which can be securely identified and correlated between cores taken from throughout the basin. The deposits range in thickness but contain a consistent and recognizable three-part stratigraphic sequence characterized by changes in grain size distributions and other physical and geochemical parameters with well-defined contacts between each sub-unit. The sedimentary framework established at this site, combined with the presence of additional suitable lakes along the fault trace and multiple paleoseismic trench datasets, provides strong potential for the future development of a highly-resolved, cross-validated, and complete postglacial paleoseismic history of the Teton fault.

Data availability statement

The raw data supporting the conclusion of this article will be made available by the authors, without undue reservation.

Author contributions

DL: Conceptualization, Data curation, Formal Analysis, Funding acquisition, Investigation, Methodology, Project administration, Resources, Supervision, Validation, Visualization, Writing–original draft, Writing–review and editing. AB: Data curation, Formal Analysis, Investigation, Methodology, Writing–original draft. SC: Conceptualization, Data curation, Formal Analysis, Investigation, Methodology, Resources, Supervision, Validation, Writing–original draft, Writing–review and editing, Project administration. AM: Data curation, Formal Analysis, Methodology, Validation, Visualization, Writing–original draft, Writing–review and editing, Investigation. MA: Data curation, Funding acquisition, Investigation, Methodology, Resources, Writing–review and editing, Project administration. AH: Data curation, Investigation, Methodology, Resources, Writing–review and editing. MP: Data curation, Investigation, Methodology, Writing–review and editing.

Conflict of interest

The authors declare that the research was conducted in the absence of any commercial or financial relationships that could be construed as a potential conflict of interest.

Publisher's note

All claims expressed in this article are solely those of the authors and do not necessarily represent those of their affiliated organizations, or those of the publisher, the editors and the reviewers. Any product that may be evaluated in this article, or claim that may be made by its manufacturer, is not guaranteed or endorsed by the publisher.

Supplementary material

The Supplementary Material for this article can be found online at: https://www.frontiersin.org/articles/10.3389/feart.2024.1391441/full#supplementary-material

References

Addison, J. A., Finney, B. P., Jaeger, J. M., Stoner, J. S., Norris, R. D., and Hangsterfer, A. (2013). Integrating satellite observations and modern climate measurements with the recent sedimentary record: an example from Southeast Alaska. *J. Geophys. Res. Oceans* 118, 3444–3461. doi:10.1002/jgrc.20243

Alexander, J., and Mulder, T. (2002). Experimental quasi-steady density currents. *Mar. Geol.* 186 (3-4), 195–210. doi:10.1016/s0025-3227(02)00313-4

Beattie, P. D., and Dade, W. B. (1996). Is scaling in turbidite deposition consistent with forcing by earthquakes? *J. Sediment. Res.* 66 (5), 909–915. doi:10.1306/d4268437-2b26-11d7-8648000102c1865d

Beck, C. (2009). Late Quaternary lacustrine paleo-seismic archives in north-western Alps: examples of earthquake-origin assessment of sedimentary disturbances. *Earth Sci. Rev.* 96, 327–344. doi:10.1016/j.earscirev.2009.07.005

Becker, A., Ferry, M., Monecke, K., Schnellmann, M., and Giardini, D. (2005). Multiarchive paleoseismic record of late Pleistocene and Holocene strong earthquakes in Switzerland. *Tectonophysics* 400 (1–4), 153–177. doi:10.1016/j.tecto.2005.03.001

Bertrand, S., Charlet, F., Chapron, E., Fagel, N., and De Batist, M. (2008). Reconstruction of the Holocene seismotectonic activity of the southern andes from seismites recorded in lago icalma, Chile, 39°S. *39°S. Palaeogeogr. Palaeoclimatol. Palaeoecol.* 259, 301–322. doi:10.1016/j.palaeo.2007.10.013

Blumm, A., Larsen, D. J., Crump, S. E., and Abbott, M. B. (2019). Characterizing earthquake generated turbidites in sediments from Jenny Lake, Grand Teton national Park, WY. *AGU Fall Meet. Abstr.* 2019, EP21C–2224.

Bouma, A. H. (2004). Key controls on the characteristics of turbidite systems. *Geol. Soc.* 222 (1), 9–22. London, Special Publications. doi:10.1144/gsl.sp.2004.222.01.02

Byrd, J. O., Smith, R. B., and Geissman, J. W. (1994). The Teton Fault, Wyoming: topographic signature, neotectonics, and mechanisms of deformation. *J. Geophys. Res.* 99 (20,099–20), 20095–20122. doi:10.1029/94jb00281

Byrd, J. O. D. (1995). *Neotectonics of the Teton Fault, Wyoming. PhD dissertation.* Salt Lake City, Utah: University of Utah, 295.

Crosby, B. (2019). A LiDAR-based landslide inventory and associated map portal (story map) for Grand Teton National Park. *UW–NPS Res. Stn. Annu. Rep.* 42, 1–4. doi:10.13001/uwnpsrc.2019.5731

Daxer, C., Ortler, M., Fabbri, S. C., Hilbe, M., Hajdas, I., Dubois, N., et al. (2022). High-resolution calibration of seismically-induced lacustrine deposits with historical earthquake data in the eastern alps (carinthia, Austria). *Quat. Sci. Rev.* 284, 107497. doi:10.1016/j.quascirev.2022.107497

DuRoss, C. B., Gold, R. D., Briggs, R. W., Delano, J. E., Ostenaa, D. A., Zellman, M., et al. (2019). Holocene earthquake history and slip rate of the southern Teton fault, Wyoming, USA. *GSA Bull.* 132 (7-8), 1566–1586. doi:10.1130/b35363.1

DuRoss, C. B., Zellman, M. S., Thackray, G. D., Briggs, R. W., Gold, R. D., and Mahan, S. A. (2020). Holocene paleoseismology of the Steamboat Mountain site: evidence for full-length rupture of the Teton Fault, Wyoming. *Bull. Seismol. Soc. Am.* 111 (1), 439–465. doi:10.1785/0120200212

Egan, J., Staff, R., and Blackford, J. (2015). A high-precision age estimate of the Holocene Plinian eruption of Mount Mazama, Oregon, USA. *Holocene* 25 (7), 1054–1067. doi:10.1177/0959683615576230

Fan, J., Xu, H., Shi, W., Guo, Q., Zhang, S., Wei, X., et al. (2022). A~ 28-kyr continuous lacustrine paleoseismic record of the intraplate, slow-slipping Fuyun Fault in northwest China. *Front. Earth Sci.* 10. doi:10.3389/feart.2022.828801

Fan, J., Zhai, D., Xu, H., Wei, X., Jin, C., Jiang, H., et al. (2023). Distinct lake sedimentary imprints of earthquakes, floods and human activities in the Xiaojiang Fault zone: towards a quantitative paleoseismograph in the southeastern Tibetan Plateau. *Sci. Total Environ.* 868, 161662. doi:10.1016/j.scitotenv.2023.161662

Goldfinger, C., Nelson, C. H., Morey, A. E., Johnson, J. E., Patton, J. R., Karabanov, E., et al. (2012). *Turbidite event history—methods and implications for Holocene paleoseismicity of the Cascadia subduction zone.* U.S. Geological Survey Professional Paper 1661–F, 170.

Hampel, A., Hetzel, R., and Erdmann, M. S. (2021). Postglacial slip distribution along the Teton normal fault (Wyoming, USA), derived from tectonically offset geomorphological features. *Geosphere* 17 (5), 1517–1533. doi:10.1130/ges02370.1

Hibsch, C., Alvarado, A., Yepes, H., Perez, V. H., and Sébrier, M. (1997). Holocene liquefaction and soft-sediment deformation in Quito (Ecuador): a paleoseismic history recorded in lacustrine sediments. *J. Geodyn.* 24 (1-4), 259–280. doi:10.1016/s0264-3707(97)00010-0

Howarth, J. D., Fitzsimons, S. J., Norris, R. J., and Jacobsen, G. E. (2012). Lake sediments record cycles of sediment flux driven by large earthquakes on the Alpine fault, New Zealand. *Geology* 40 (12), 1091–1094. doi:10.1130/G33486.1

Johnson, S. E., Swallom, M. L., Thigpen, R., McGlue, M., Dortch, J. M., Gallen, S., et al. (2022). The influence of glacial topography on fluvial efficiency in the Teton Range, Wyoming (USA). *Earth Planet. Sci. Lett.* 592, 117643. doi:10.1016/j.epsl.2022.117643

Kuehn, S. C., Froese, D. G., Carrara, P. E., Foit, F. F., Jr., Pearce, N. J. G., and Rotheisler, P. (2009). Major- and trace-element characterization, expanded distribution, and a new

chronology for the latest Pleistocene Glacier Peak tephras in western North America. *Quat. Res.* 71, 201–216. doi:10.1016/j.yqres.2008.11.003

Larsen, D. J., Crump, S. E., Abbott, M. B., Harbert, W., Blumm, A., Wattrus, N. J., et al. (2019). Paleoseismic evidence for climatic and magmatic controls on the Teton Fault, WY. *Geophys. Res. Lett.* 46, 13036–13043. doi:10.1029/2019GL085475

Larsen, D. J., Finkenbinder, M. S., Abbott, M. B., and Ofstun, A. R. (2016). Deglaciation and postglacial environmental changes in the Teton mountain range recorded at Jenny Lake, Grand Teton national Park, WY. *Quat. Sci. Rev.* 138, 62–75. doi:10.1016/j.quascirev.2016.02.024

Lê, S., Josse, J., and Husson, F. (2008). FactoMineR: an R package for multivariate analysis. *J. Stat. Softw.* 25, 1–18. doi:10.18637/jss.v025.i01

Leithold, E. L., Wegmann, K. W., Bohnenstiehl, D. R., Joyner, C. N., and Pollen, A. F. (2019). Repeated megaturbidite deposition in lake crescent, Washington, USA, triggered by Holocene ruptures of the lake creek-boundary Creek fault system. *Bull. Geol. Soc. Am.* 131, 2039–2055. doi:10.1130/B35076.1

Licciardi, J. M., and Pierce, K. L. (2008). Cosmogenic exposure-age chronologies of Pinedale and bull lake glaciations in greater yellowstone and the Teton range, USA. *Quat. Sci. Rev.* 27, 814–831. doi:10.1016/j.quascirev.2007.12.005

Licciardi, J. M., and Pierce, K. L. (2018). History and dynamics of the greater yellowstone glacial system during the last two glaciations. *Quat. Sci. Rev.* 200, 1–33. doi:10.1016/j.quascirev.2018.08.027

Love, J. D., Reed, J. C., Jr., and Christiansen, A. C. (1992). Geologic map of Grand Teton national Park, Teton county, Wyoming. *U. S. Geol. Surv. Misc. Investig. Ser. MAP I-2031.*

Machette, M. N., Pierce, K. L., McCalpin, J. P., Haller, K. M., and Dart, R. L. (2001). Map and data for Quaternary faults and folds in Wyoming. *U. S. Geol. Surv. Open-File Rep.* 521, 154. 01-461.

Maloney, J. M., Noble, P. J., Driscoll, N. W., Kent, G. M., Smith, S. B., Schmauder, G. C., et al. (2013). Paleoseismic history of the fallen leaf segment of the west tahoe–dollar point fault reconstructed from slide deposits in the lake tahoe basin, California-Nevada. *Geosphere* 9, 1065–1090. doi:10.1130/ges00877.1

Moernaut, J., Van Daele, M., Fontijn, K., Heirman, K., Kempf, P., Pino, M., et al. (2018). Larger earthquakes recur more periodically: new insights in the megathrust earthquake cycle from lacustrine turbidite records in south-central Chile. *Earth Planet. Sci. Lett.* 481, 9–19. doi:10.1016/j.epsl.2017.10.016

Moernaut, J., Van Daele, M., Heirman, K., Fontijn, K., Strasser, M., Pino, M., et al. (2014). Lacustrine turbidites as a tool for quantitative earthquake reconstruction: new evidence for a variable rupture mode in south central Chile. *J. Geophys. Res. Solid Earth* 119, 1607–1633. doi:10.1002/2013JB010738

Moernaut, J., Van Daele, M., Strasser, M., Clare, M. A., Heirman, K., Viel, M., et al. (2017). Lacustrine turbidites produced by surficial slope sediment remobilization: a mechanism for continuous and sensitive turbidite paleoseismic records. *Mar. Geol.* 384, 159–176. doi:10.1016/j.margeo.2015.10.009

Morey, A. E., Goldfinger, C., Briles, C. E., Gavin, D. G., Colombaroli, D., and Kusler, J. E. (2013). Are great Cascadia earthquakes recorded in the sedimentary records from small forearc lakes? *Nat. Hazards Earth Syst. Sci.* 13, 2441–2463. doi:10.5194/nhess-13-2441-2013

Mulder, T., and Alexander, J. (2001). The physical character of subaqueous sedimentary density flows and their deposits. *Sedimentology* 48 (2), 269–299. doi:10.1046/j.1365-3091.2001.00360.x

Mulder, T., and Chapron, E. (2011). *Flood deposits in continental and marine environments: character and significance.* doi:10.1306/13271348St613436

Mulder, T., Syvitski, J. P., Migeon, S., Faugères, J. C., and Savoye, B. (2003). Marine hyperpycnal flows: initiation, behavior and related deposits. A review. *Mar. Petroleum Geol.* 20 (6-8), 861–882. doi:10.1016/j.marpetgeo.2003.01.003

Pierce, K. L., and Good, J. D. (1992). *Field guide to the quaternary geology of Jackson Hole, Wyoming (No. 92-504).* US Geological Survey. US Dept. of the Interior.

Pierce, K. L., Licciardi, J. M., Good, J. M., and Jaworowski, C. (2018). Pleistocene glaciation of the Jackson Hole area, Wyoming, *Wyo. U.S. Geol. Surv. Prof. Pap.* 1835, 56. doi:10.3133/pp1835

Praet, N., Van Daele, M., Collart, T., Moernaut, J., Vandekerkhove, E., Kempf, P., et al. (2020). Turbidite stratigraphy in proglacial lakes: deciphering trigger mechanisms using a statistical approach. *Sedimentology* 67 (5), 2332–2359. doi:10.1111/sed.12703

Rodriguez-Pascua, M., De Vicente, G., Calvo, J. P., and Pérez-López, R. (2003). Similarities between recent seismic activity and paleoseismites during the late miocene in the external Betic Chain (Spain): relationship by 'b'value and the fractal dimension. *J. Struct. Geol.* 25 (5), 749–763. doi:10.1016/s0191-8141(02)00078-0

Sabatier, P., Moernaut, J., Bertrand, S., Van Daele, M., Kremer, K., Chaumillon, E., et al. (2022). A review of event deposits in lake sediments. *Quaternary* 5 (3), 34. doi:10.3390/quat5030034

Smith, R. B., Byrd, J. O. D., and Susong, D. D. (1993). "The Teton fault, Wyoming: seismotectonics, Quaternary history, and earthquake hazards,". *Geology of Wyoming*. Editors A. W. Snoke, J. R. Steidtmann, and S. M. Roberts (Laramie, Wyoming: Geological Survey of Wyoming, Memoir), 5, 628–667.

Smith, S. B., Karlin, R. E., Kent, G. M., Seitz, G. G., and Driscoll, N. W. (2013). Holocene subaqueous paleoseismology of lake tahoe. *GSA Bull.* 125 (5-6), 691–708. doi:10.1130/b30629.1

St-Onge, G., Mulder, T., Piper, D. J., Hillaire-Marcel, C., and Stoner, J. S. (2004). Earthquake and flood-induced turbidites in the saguenay fjord (québec): a Holocene paleoseismicity record. *Quat. Sci. Rev.* 23 (3-4), 283–294. doi:10.1016/j.quascirev.2003.03.001

Strasser, M., Anselmetti, F. S., Fah, D., Giardini, D., and Schnellmann, M. (2006). Magnitudes and source areas of large prehistoric northern Alpine earthquakes revealed by slope failures in lakes. *Geology* 34, 1005–1008. doi:10.1130/g22784a.1

Strasser, M., Monecke, K., Schnellmann, M., and Anselmetti, F. S. (2013). Lake sediments as natural seismographs: a compiled record of Late Quaternary earthquakes in Central Switzerland and its implication for Alpine deformation. *Sedimentology* 60, 319–341. doi:10.1111/sed.12003

Strasser, M., Stegmann, S., Bussmann, F., Anselmetti, F. S., Rick, B., and Kopf, A. (2007). Quantifying subaqueous slope stability during seismic shaking: lake Lucerne as model for ocean margins. *Mar. Geol.* 240, 77–97. doi:10.1016/j.margeo.2007.02.016

Thackray, G. D., and Staley, A. E. (2017). Systematic variation of Late Pleistocene fault scarp height in the Teton Range, Wyoming, USA: variable fault slip rates or variable landform ages? *Geosphere* 13, 287–300. doi:10.1130/GES01320.1

Tranel, L. M., Spotila, J. A., Binnie, S. A., and Freeman, S. P. (2015). Quantifying variable erosion rates to understand the coupling of surface processes in the Teton Range, Wyoming. *Geomorphology* 228, 409–420. doi:10.1016/j.geomorph.2014.08.018

Van Daele, M., Araya-Cornejo, C., Pille, T., Vanneste, K., Moernaut, J., Schmidt, S., et al. (2019). Distinguishing intraplate from megathrust earthquakes using lacustrine turbidites. *Geology* 47, 127–130. doi:10.1130/g45662.1

Van Daele, M., Moernaut, J., Doom, L., Boes, E., Fontijn, K., Heirman, K., et al. (2015). A comparison of the sedimentary records of the 1960 and 2010 great Chilean earthquakes in 17 lakes: implications for quantitative lacustrine palaeoseismology. *Sedimentology* 62, 1466–1496. doi:10.1111/sed.12193

Vandekerkhove, E., Van Daele, M., Praet, N., Cnudde, V., Haeussler, P. J., and De Batist, M. (2020). Flood-triggered versus earthquake-triggered turbidites: a sedimentological study in clastic lake sediments (Eklutna Lake, Alaska). *Sedimentology* 67 (1), 364–389. doi:10.1111/sed.12646

Wentworth, C. K. (1922). A scale of grade and class terms for clastic sediments. *J. Geol.* 30, 377–392. doi:10.1086/622910

White, B. J. P., Smith, R. B., Husen, S., Farrell, J. M., and Wong, I. (2009). Seismicity and earthquake hazard analysis of the Teton–Yellowstone region, Wyoming. *J. Volcanol. Geotherm. Res.* 188, 277–296. doi:10.1016/j.jvolgeores.2009.08.015

Wilhelm, B., Nomade, J., Crouzet, C., Litty, C., Sabatier, P., Belle, S., et al. (2016). Quantified sensitivity of small lake sediments to record historic earthquakes: implications for paleoseismology. *J. Geophys. Res. Earth Surf.* 121, 2–16. doi:10.1002/2015JF003644

Zellman, M., DuRoss, C. B., Thackray, G. R., Personius, S. F., Reitman, N. G., Mahan, S. A., et al. (2020b). Holocene rupture history of the central Teton fault at Leigh Lake; Grand Teton national Park, Wyoming. *Bull. Seismol. Soc. Am.* 132, 67–82. doi:10.1785/0120190129

Zellman, M. S., DuRoss, C. B., Gold, R. D., Thackray, G. D., Wittke, S. J., Delano, J. E., et al. (2020a). Does the Phillips Valley fault rupture with the Teton fault? (abstract). *Seismol. Res. Lett.* 91 (2B), 1192.

Zellman, M. S., DuRoss, C. B., and Thackray, G. D. (2019). *The Teton fault:, Wyoming geological Survey open-file report 2019-1, scale 1:75,000.*